Loschmidt echo and momentum distribution in a Kitaev spin chain

Vimalesh Kumar Vimal [1,*] H. Wanare,[1,†] and V. Subrahmanyam [2,‡]
[1]*Department of Physics, Indian Institute of Technology, Kanpur 208016, India*
[2]*School of Physics, University of Hyderabad Gachibowli, Hyderabad 500046, India*

(Received 11 April 2022; accepted 6 September 2022; published 28 September 2022)

We investigate the Loschmidt echo in a one-dimensional spin chain having Kitaev-type interaction in constant and kicked magnetic fields. The Loschmidt echo for the initial states having different magnon excitations shows long-time revivals for smaller chains and has short-time revival peaks for the longer chains. The system near the critical point shows peculiarly long-time revival peaks of the Loschmidt echo for relatively larger chains. The presence of a magnon in the initial state affects the Loschmidt echo revival peaks. The momentum distribution function exhibits maxima for a few momenta that are associated with the momentum of the magnon excitation present in the initial states. The probability maxima decay as $O(1/N)$ with the system size. For the Hamiltonian with kicked magnetic fields, the Loschmidt echo depends on the kick period. For a special kick period, the Loschmidt echo shows no evolution at all irrespective of the system size.

DOI: 10.1103/PhysRevA.106.032221

I. INTRODUCTION

The recent experimental advancement in ultracold atoms trapped on the optical lattices [1,2] has created a renewed interest in exploring the dynamics of quantum systems, particularly using quantum quenches [3–7]. For closed quantum systems, the quantum quenching leads to a unitary evolution which can be determined by the Loschmidt echo analysis [8–10]. For the quantum systems quenched to the critical point, the dynamics of the finite chains have periodic revival peak structures which decrease with the increasing system size [10–19]. The enhanced decay of the Loschmidt echo (LE) can be considered as the witness of the quantum phase transition [20–23]. The singularities of LE can also give the signature of strongly localized phases [24]. The extensions of the LE have also been used to study information scrambling, and the direct link between the out-of-time-order correlator and the Loschmidt echo has been studied [25–27]. In this process, the local information of the system disperses to the nonlocal degrees of the freedom throughout the system [28–34]. The Loschmidt echo can be computed by taking the overlap of the prior to and after the quenched state that can be tuned using the Hamiltonian parameters. The rate function defined using the LE has been studied extensively to trace the signal of the dynamical phase transition in many quantum systems [35–49]. In recent times, the connection between the quantum quenches and the topological properties and topological edge states has also been investigated. The topological systems, especially the topological superconductor, have been investigated in detail [50–52] and have been shown to be quite robust to the quantum quenching [53–55].

The concept of the Loschmidt echo in the physical system was first implemented in the nuclear magnetic resonance (NMR) experiment [56] by applying radio-frequency pulses to an ensemble of spins under a static magnetic field. After a certain time, determined by these pulses, the nuclear induction signal called spin echo was observed. The experimental results were shown where a suitable sequence of radio-frequency pulses was used to show that the nuclear spin Hamiltonian evolves back in time and the revival of magnetization can be obtained in the system [57]. Further, polarization echo [58] was shown, where a local excitation injected in a many-body system is partially observed after the forward and reverse evolution. The difficulty encountered in experimental errors and reversibility time of the LE has been studied recently [59,60].

We study the Loschmidt echo in a Kitaev spin chain in one dimension [61–63] when the Hamiltonians are set at different global parameters. We will study the behavior of the LE both near and away from the critical region. We will examine initial states with no magnon excitation and initial states with one-magnon excitations.

We also study the momentum distribution of an excited magnon for this model within the framework of the LE. The momentum distribution has been studied in different scenarios. The momentum distribution in spinless bosons [66] and in spin-1 bosons [67] in one dimension have been studied previously. Also, the signature of the Fulde-Ferrel-Larkin-Ochnikov (FFLO) phase can be seen in the momentum distribution function of the trapped one-dimensional Fermi gases [64,65]. The momentum distribution function can give information about the spatial distribution of electrons in the quasiparticle bands [68]. In the momentum space, it can give the probabilistic distribution of a magnon excitation in the time-evolved state of the Hamiltonian. We will see that the evolution characteristic of the momentum distribution coincides with the characteristic of the LE dynamics.

*vimalkv@iitk.ac.in
†hwanare@iitk.ac.in
‡vmani@iitk.ac.in

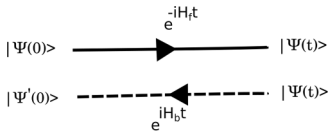

FIG. 1. Loschmidt echo.

Also, the peaks of the distribution function are confined to some special values of momenta, which is expected in this case.

The Loschmidt echo measures the degree of reversibility of the system when it evolves under a Hamiltonian for a certain amount of time and evolves back using the perturbed Hamiltonian for the same amount of time. The forward and backward evolution in time is shown pictorially in Fig. 1. The Loschmidt echo (LE) is defined as the square of the modulus of overlap of the two states that evolve from the same initial state under the considered Hamiltonian and Hamiltonian with perturbation [69]. An initial state $|\psi(0)\rangle$ evolves under the Hamiltonian H_f for time t and then it further evolves under the Hamiltonian $-H_b$ for the same time. This can be written as

$$\mathsf{L}(t) = |\,\langle\psi(0)|\,e^{iH_b t}e^{-iH_f t}\,|\psi(0)\rangle\,|^2. \tag{1}$$

From this, LE can be viewed as a measure of the degree of the reversibility of the dynamics. In this paper, we investigate the LE for three different initial states which evolve under the Hamiltonians H_f and H_b, which are set on and off the critical point by tuning the Hamiltonian parameters. The paper is organized in the following form. Section II discusses the Hamiltonian setup, its eigenstates, and the state dynamics. Section III discusses the LE for a zero-magnon initial state. The LE for one magnon in the momentum space is discussed in Sec. IV. In Sec. V, we discuss the LE for an initial state with a uniform probability distribution of momenta. We consider a kicked magnetic field in the Hamiltonian and discuss the LE and the momentum distribution in all three initial states in Sec. VI. We conclude with the results in Sec. VII.

II. EIGENSTATES OF THE HAMILTONIAN

We consider a system of N spins in one dimension having nearest-neighbor interactions in the presence of a transverse magnetic field. The nearest spins have a Kitaev-type interaction, which is an $x-x$ interaction on the odd pair of sites and $y-y$ interactions on the even pair of sites. The spin chain Hamiltonian considered here is the one-dimensional simplification of the two-dimensional Kitaev honeycomb lattice model [70,71]. The $z-z$ interaction in the Kitaev honeycomb Hamiltonian is replaced by the uniform magnetic field term. The spin chain Hamiltonian is given by

$$H = j_x\sum_{i=\text{odd}}^{N-1}\sigma_i^x\sigma_{i+1}^x + j_y\sum_{i=\text{even}}^{N}\sigma_i^y\sigma_{i+1}^y + h\sum_{i=1}^{N}\sigma_i^z. \tag{2}$$

The coefficient j_x (j_y) is the strength of the nearest-neighbor interaction on the odd (even) pair of sites. The coefficient h is the strength of the uniform magnetic field in the system. The spin model cannot be simplified to the Ising or the xy spin chains because a spin at any site in this model has only one, either x or y, direction of interaction with its next-nearest neighbor. For this reason, it cannot be mapped into the Ising or the XY spin models. The presence of only one degree of interaction at each site adds surprising features to this model, some of which are contrary to the one-dimensional behavior. The Hamiltonian has a macroscopic degeneracy in the ground state in the absence of the magnetic field. However, the ground-state quantum correlation measures like the concurrence measure of the entanglement, and the quantum discord does not show an expected scaling behavior near the critical point of the system. The Hamiltonian is diagonalizable using the Jordan-Wigner fermion method, and all the eigenstates can be constructed, and the dynamics can be studied [61–63]. We will represent the Hamiltonian parameters in the unit of j_x, effectively making it a two-parameter family of $r = j_y/j_x$, and h/j_x. Thus, we will represent the Hamiltonian as $H = H(r, h/j_x)$ in the following. We will briefly review how to study the dynamics of an initial state using this Hamiltonian. In the momentum space, the Hamiltonian takes the form $H = 2\sum_q H_q$, where the sum is over $N/4$ momentum values, $0 < q < \pi/2$. Each q is associated with the four momentum values $q-\pi$, $-q$, q, and $\pi - q$. The free fermion form of H_q can be written as

$$H_q = \sum_{i=1}^{4}\lambda_i\xi_i^\dagger\xi_i. \tag{3}$$

Here, $\lambda_i = \pm|e| \pm \sqrt{|e|^2+h^2}$ are the eigenvalues of the mode Hamiltonian. The parameter $|e| = \frac{1}{2}\sqrt{[(j_x+j_y)\cos q]^2+[(j_x-j_y)\sin q]^2}$. The index i in increasing order implies the increasing values of λ_i. The operators ξ_i are the eigenoperators corresponding to λ_i, which can be written as

$$\begin{bmatrix}\xi_1^\dagger\\ \xi_2^\dagger\\ \xi_3^\dagger\\ \xi_4^\dagger\end{bmatrix} = \begin{bmatrix}\mathcal{C} & i\mathcal{S} & h_1\mathcal{C} & ih_1\mathcal{S}\\ \mathcal{S} & -i\mathcal{C} & h_2\mathcal{S} & -ih_2\mathcal{C}\\ \mathcal{C} & i\mathcal{S} & h_3\mathcal{C} & ih_3\mathcal{S}\\ \mathcal{S} & -i\mathcal{C} & h_4\mathcal{S} & -ih_4\mathcal{C}\end{bmatrix}\begin{bmatrix}F_+^\dagger\\ G_+^\dagger\\ F_-^\dagger\\ G_-^\dagger\end{bmatrix}. \tag{4}$$

Here, $\mathcal{C} = \cos\theta_q/2$, $\mathcal{S} = \sin\theta_q/2$ with $\theta_q = \sin^{-1}\frac{(1-r)\sin q}{\sqrt{[(1+r)\cos q]^2+[(1-r)\sin q]^2}}$, and $h_i = h/\lambda_i$. The fermion operators $F_\pm = (c_{q-\pi} - c_{-q}^\dagger)/\sqrt{2}$ and $G_\pm = (c_q - c_{\pi-q}^\dagger)/\sqrt{2}$. Using Eq. (3), all the eigenstates of the Hamiltonian can be created from the vacuum state defined as $\xi_i\,|\text{vac}\rangle = 0$. The unnormalized ground state can be written as

$$\begin{aligned}|g\rangle = \prod_{0\leqslant q\leqslant\pi/2}\,&[(1-h_1)(1-h_2) + \{(1-h_1h_2) + (h_2-h_1)\\ &\times\cos\theta_q\}c_q^\dagger c_{\pi-q}^\dagger - i(h_1-h_2)\sin\theta_q(c_{-q}^\dagger c_q^\dagger + c_{q-\pi}^\dagger c_{\pi-q}^\dagger)\\ &+ \{(1-h_1h_2) - (h_2-h_1)\cos\theta_q\}c_{q-\pi}^\dagger c_q^\dagger + (1+h_1)\\ &\times(1+h_2)c_{q-\pi}^\dagger c_{-q}^\dagger c_q^\dagger c_{\pi-q}^\dagger]\,|0000\rangle.\end{aligned} \tag{5}$$

Similarly, we can construct the excited states using the mode operators $\xi_i^\dagger$ on the vacuum state for different q values. In the absence of magnetic field, there are mode operators with zero energy. The presence of the zero-energy eigenoperators causes the Hamiltonian to have a macroscopic degeneracy

in its ground state. The quantum correlations also have surprising features in this model. Contrary to the Ising and xy spin chains, the quantum correlations such as the concurrence measure and the quantum discord do not exhibit a signal of the quantum critical point in the system. However, these correlations show maxima at the quantum critical point [61]. The dynamics of magnetization shows counterintuitive revivals with respect to the concurrence and the quantum discords [62]. In the following sections, we will consider different initial states and investigate the LE and the evolution of the momentum distribution.

III. NO-MAGNON INITIAL STATE

We consider an initial state of spins completely polarized in the $-ve$ z axis, which translates to a zero-fermion state in the momentum space. The state is written as $|\psi(0)\rangle = |00..00\rangle$. This state can be thought of as an eigenstate of the Hamiltonian in Eq. (2) when the magnetic field is very large. According to the protocol discussed in Eq. (1), we can write the forward evolution as

$$|\psi(t)\rangle = e^{-iH_f t}\,|00..00\rangle\,. \tag{6}$$

In the above expression, $H_f = H(r, h_f/j_x)$ represents the forward Hamiltonian with h_f, the magnetic field. It can be written as the sum of the mode Hamiltonians H_q [shown in Eq. (3)] that commute with each other, $H_f = 2\sum_q H_q$. Thus, the forward evolution can be further written as

$$|\psi(t)\rangle = e^{-2i\sum_q H_q t}\,|00..00\rangle = \Pi_q\,|\phi_q(t)\rangle\,. \tag{7}$$

Here, $|\phi_q(t)\rangle \equiv e^{-2iH_q t}\,|0000\rangle_q$ evolves under the mode Hamiltonian H_q in the forward direction. Similarly, the backward evolution happens under the Hamiltonian $H_b = H(r, h_b/j_x)$, where h_b is the magnetic field for this evolution. The Hamiltonian can be written as $H_b = 2\sum_q H'_q$. Here, H'_q are the mode Hamiltonians of H_b. The time-evolved state can be written as

$$|\psi'(t)\rangle = e^{-2i\sum_q H'_q t}\,|00..00\rangle \equiv \Pi_q\,|\phi'_q(t)\rangle\,, \tag{8}$$

where the state $|\phi'_q(t)\rangle = e^{-2iH'_q t}\,|0000\rangle_q$ evolves under the mode Hamiltonian H'_q in the reverse direction. Therefore, the LE in Eq. (1) can be simplified as the square of amplitude of the overlap of the two states $|\psi(t)\rangle$ and $|\psi'(t)\rangle$, given as

$$\mathsf{L}(t) = |A|^2, \quad A = \Pi_q A_q, \quad A_q = \langle\phi'_q(t)|\phi_q(t)\rangle\,. \tag{9}$$

Using Eq. (5) and its equivalent for the excited states, we can calculate the LE echo as a function of time for different magnetic field values for the forward and reverse directions. In Fig. 2, LE is plotted when forward evolution happens under the Hamiltonian $H_f(r = 1, h_f/j_x = 1)$ and reverse evolution happens by flipping the magnetic field direction, $H_b(r = 1, h_b/j_x = -1)$. Throughout the analysis, the local interaction j_x is set to unity. The Loschmidt echo for small chains has a periodic structure in the evolution, while for longer spin chains, its revival peaks are reduced. Figure 2(a) shows the behavior of the Loschmidt echo for the smaller spin chains, while Fig. 2(b) shows the same for the larger chain lengths. The LE at $t = 0$ is unity as the system is in its initial state. As time progresses, the LE decays exponentially in a very short time. However, it revives quickly and a periodic

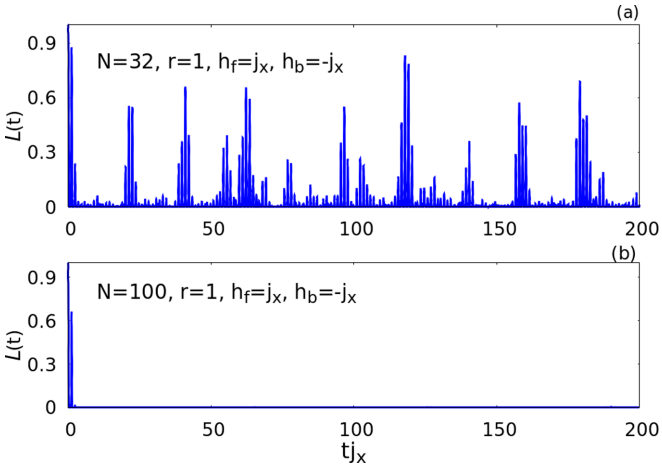

FIG. 2. LE as a function of time for (a) a shorter chain of $N = 32$ and (b) a larger chain of $N = 100$. The forward evolutions in both cases are at $r = 1$ and $h_f/j_x = 1$, while for the reverse evolution, the magnetic field is flipped. The Loschmidt echo shows long-time revival peaks for smaller chains. For the larger spin chains, it decays exponentially and has only short-time revival peaks.

structure of dynamics appears over time. Revival peaks appear only for shorter chain lengths in a long-time evolution, as shown in Fig. 2(a). For up to $N = 44$, the LE shows periodic revival peaks in the long-time evolution, but as the length of the chain increases, these peaks start vanishing. In Fig. 2(b), for $N = 100$, only one peak is significant, which appears soon after the evolution, and no further significant revival peaks are seen in the long-time evolution. For larger spin chains, A_q functions in Eq. (9) go out of phase quickly after the evolution, making the Loschmidt echo difficult to revive in long-time evolution. We can also analyze the LE behavior at different r values. At $r = 0$, $h_f = 1$, $h_b = -1$, the LE shows periodic behavior as a function of time. This could be because, at $r = 0$, all A_q functions are periodic and remain in phase over time. As we increase r from 0 to 1, the LE loses its periodic nature and falls to zero, and does not revive. We plot the LE as a function of time for different number of sites in Fig. 3. At $r = 1$ and $h_f = 1$, $h_b = -1$, the LE shows revival peaks for different chain lengths. The strong and periodic revival peaks in the short-length chains indicate that it is easy to align the spins of the system in the z direction. However, since all spin-up or spin-down states are not the eigenstates of the system, the LE cannot show a perfect revival. For larger chains, the short-time peak falls to 0.1 for $N = 500$. Beyond that, it becomes comparatively insignificant and the Loschmidt echo exhibits no short- or long-time revival peaks at all in the thermodynamic limit. The evolution of the rate function of the Loschmidt echo in the Kitaev honeycomb model in the presence of the magnetic field has similar characteristics. For this behavior, the honeycomb Hamiltonian is set to have zero spin-spin interaction in the z direction, $J_z = 0$, and the quench does not cross the phase [36]. In this setup, the honeycomb model is similar to our Hamiltonian except for the magnetic field, which is applied in all three spin directions.

When the evolution in either direction happens under the Hamiltonian near the critical point, the revival peaks of the

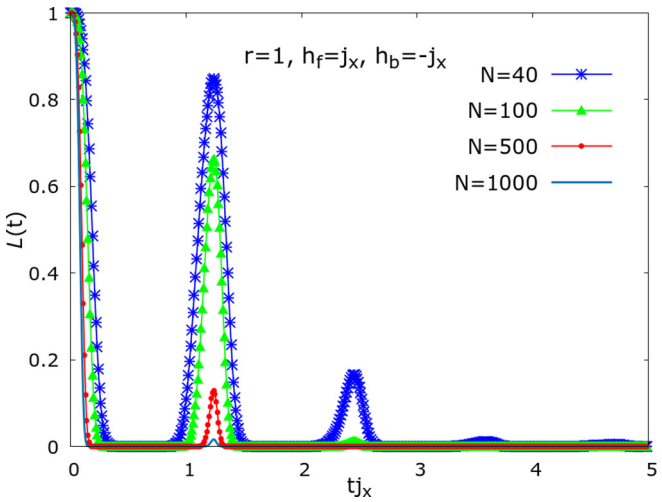

FIG. 3. LE as a function of N for $r = 1$ and $h_f = j_x, h_b = -j_x$. After $N = 40$, a strong short-time revival peak appears, which remains significant up to $N = 500$. Beyond this, the Loschmidt echo in the thermodynamic limit has no long- or short-time revival peaks.

Loschmidt echo are gone completely, even for smaller spin chains. Figure 4 shows the behavior of LE for the different spin chains in such a scenario. The LE for a $N = 32$ spin chain is plotted in Fig. 4(a). We set $r = 1$ and the forward magnetic field, $h_f = 0$, and consider different magnetic fields h_b when the system evolves backward in time. We can see that as we increase h_b, the LE falls very sharply and never revives. In Fig. 4(b), the LE has been plotted for $h_b = -0.5 j_x$, keeping other parameters the same as they are in Fig. 2(a). We can see that the LE shows polynomial decay for small spin chains, while it shows a sudden fall for large spin chains. Therefore, we show only short-time dynamics for these two cases. In Fig. 4(c), we have shown the behavior of LE for larger lengths $N = 100$ and $N = 120$ in the critical region $h_f = 0.1 j_x$ and $h_b = -0.1 j_x$. In this case, the Loschmidt echo exhibits revival peaks after a long-time evolution. However, these peaks sharply fall beyond these lengths. For smaller size chains, the LE exhibits periodic revival peaks with higher amplitudes. The quick revival peak that we see in a noncritical regime is not present in this case. However, the long-time revivals of the Loschmidt echo are pronounced only at $h_f = -h_b = 0.1 j_x$, which disappears as we tune the magnetic field even slightly to $h_f = -h_b = 0.15 j_x$. The magnetic fields near the critical point will show very fluctuating behavior, as expected. Also, in this case, the revival does not occur at nearly the same time for the different lengths of the chain, as it occurs for the short-time revival peak in the noncritical Hamiltonian cases. This may induce the behavior that the values of the revival peaks as a function of N do not show any certain characteristics in this case. However, for chains larger than $N = 100$, the peaks fall very quickly and become insignificant, which is the general character of the system. In a different scenario of a two-level system surrounded by the Ising-type spin chain, the time of the revival peaks has been shown to be proportional to the length of the chain [11]. They also show that the enhanced decay of LE can be used to witness quantum criticality.

IV. ONE-MAGNON INITIAL STATE WITH A DEFINITE MOMENTUM

In the last section, we have studied the even-number magnon state starting from the zero-magnon initial state. In this section, we will consider the odd-number magnon state in evolution, starting with a one-magnon initial state. Let us consider an initial state that has only one magnon with a definite momentum q, given by

$$|\psi_q(0)\rangle = c_q^\dagger |00..00\rangle . \tag{10}$$

This state will evolve into a superposition of states with different odd number of magnons. The evolution of this state can be written using the evolution of $c_q^\dagger$ under the Hamiltonian H_f, defined for Eq. (6) as

$$|\psi_q(t)\rangle = c_q^\dagger(-t) e^{-iH_f t} |00..00\rangle , \tag{11}$$

where the time evolution of the creation operator is written as

$$c_q^\dagger(-t) = e^{iH_f t} c_q^\dagger e^{-iH_f t} . \tag{12}$$

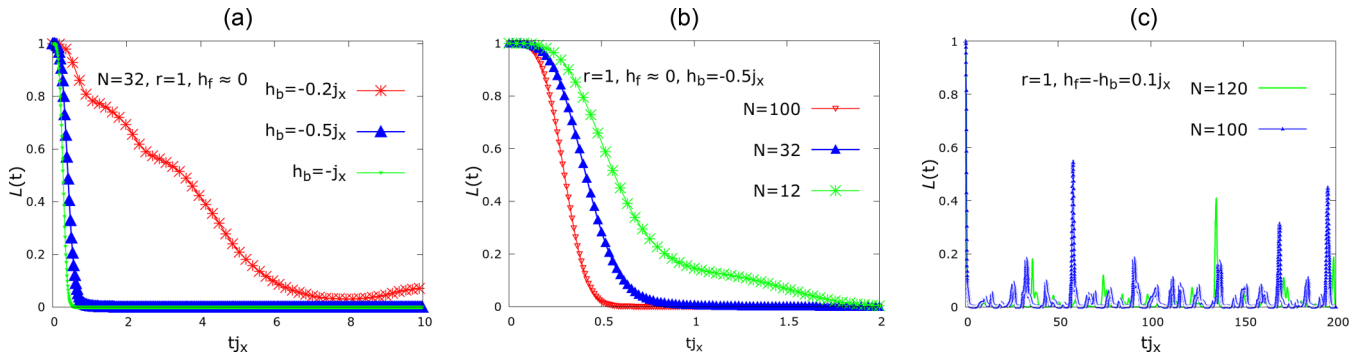

FIG. 4. Loschmidt echo near the critical point. (a) For a small chain of $N = 32$ at $r = 1$, $h_f = 0$, and different values of h_b. The Loschmidt echo decays very sharply in the higher magnetic field in the reverse evolution. (b) At $r = 1$, $h_f = 0$, and $h_b = -0.5 j_x$ for different spin chains. The LE falls more quickly and does not show revival for the longer spin chains. The revival peaks are present for the smaller chains, which we do not show in the plot. As the length of the spin chain increases beyond $N = 16$, the revival is not possible. (c) For $h_f = -h_b = 0.1 j_x$, the LE shows peaks after a long-time evolution even for larger spin chains, $N = 100$ and $N = 120$. Beyond this length, the revivals peaks fall quickly. For the smaller chains, the revivals peaks are periodic with higher amplitudes.

The time-evolution term $e^{-iH_f t}\,|00..00\rangle$ in Eq. (11) can be computed using Eq. (7). The state $|\psi_q(t)\rangle$ can further evolve under the Hamiltonian H_b. The time-evolved creation operator $c_q^\dagger(-t)$ of mode q is a function of the momentum values $\{q-\pi, -q, q, \pi-q\}$. There are $N/4$ such momentum values allowed for the Hamiltonian, which each having four modes. Therefore, $C(k,q)$ can have three more possibilities with $\{k = q-\pi, -q, \pi-q\}$. Thus, $c_q^\dagger(-t)$ can be written in terms of the other associated momenta operators as

$$c_q^\dagger(-t) = \beta_1 c_{q-\pi}^\dagger + \beta_2 c_{-q} + \beta_3 c_q^\dagger + \beta_4 c_{\pi-q}, \tag{13}$$

where $\beta_j = \sum_{i=1}^4 e^{-2i\lambda_i t}\Gamma_{i3}^*\Gamma_{ij}$. λ_i are the eigenvalues of the Hamiltonian H_q and the Γ matrix is written as

$$\Gamma = \begin{bmatrix} (1+h_1)\mathcal{C} & (1-h_1)\mathcal{S} & i(1+h_1)\mathcal{C} & i(1-h_1)\mathcal{S} \\ (1+h_2)\mathcal{S} & (1-h_2)\mathcal{C} & -i(1+h_2)\mathcal{S} & -i(1-h_2)\mathcal{C} \\ (1+h_3)\mathcal{C} & (1-h_3)\mathcal{S} & i(1+h_3)\mathcal{C} & i(1-h_3)\mathcal{S} \\ (1+h_4)\mathcal{S} & (1-h_4)\mathcal{C} & -i(1+h_4)\mathcal{S} & -i(1-h_4)\mathcal{C} \end{bmatrix}. \tag{14}$$

Thus the time-evolved mode operators in Eq. (12) are functions of all four momenta operators associated with the corresponding mode. During the course of the evolution, the probability distribution of the momentum may change. Therefore, we can overlap the final evolved state with the same or a different momentum state defined in Eq. (10). This can be written by defining a probability distribution function $P_q(k,t)$, which is essentially a momentum distribution function of the momentum k in the time-evolved state which has the initial state with a definite momentum q. This can be rewritten as

$$P_q(k,t) = \langle\psi'(t)|\, c_k'(-t) c_q^\dagger(-t)\,|\psi(t)\rangle\,, \tag{15}$$

where the $|\psi'(t)\rangle$ is defined in Eq. (8). The operator $c_k'(-t) = e^{iH_b t} c_q^\dagger e^{-iH_b t}$ defined for the backward evolution gives the time evolution of the momentum k under the Hamiltonian H_b. The time-evolved momentum operator $c_q^\dagger(-t)$ acts only on $|\phi_q(t\rangle)$, leaving other mode states of $|\psi(t)\rangle$ unaffected. Similarly, $c_k'(-t)$ acts only on $\langle\phi_q'(t|)$, leaving other mode states of $\langle\psi'(t)|$ unaffected. Therefore, we can rewrite the probability distribution function of a momentum k as

$$P_q(k,t) = |A/A_q|^2 |C(k,q)|^2, \tag{16}$$

where A and A_q are defined in Eq. (9) and

$$C(k,q) = \langle\phi_q'(t)|\, c_k'(-t) c_q^\dagger(-t)\,|\phi_q(t)\rangle\,. \tag{17}$$

The probability distribution function for $k = 1$ is just the Loschmidt echo. Therefore, the expression can be given by

$$\mathsf{L}(t) = |A/A_q|^2 |C(q,q)|^2. \tag{18}$$

We can see in the above that the presence of a magnon with a fixed momentum value in the initial state affects only the mode state associated with that momentum. Therefore, the LE for larger spin chains does not show the effect of the excitation in the initial state and has a similar result to the LE for the no-magnon initial state. However, it has a significant impact on the smaller chains. In Fig. 5, we plot the Loschmidt echo for a spin chain of $N = 32$ for the short- and the long-time evolution. The Hamiltonian parameters are set as $r = 1$, $h_f = j_x, h_b = -j_x$. The revival peaks get a little stronger by the presence of the magnon in the initial state. However, when the Hamiltonian is set in the critical zone for either direction of the evolution, the revival characteristic is lost and does not show similar behavior of the LE having no-magnon excitation in the initial state. To see the impact of the presence of one-magnon excitation in the initial state on the LE, we plot the time-averaged LE as a function of spin length in Fig. 6. The average value of LE is calculated for a long-time evolved function up to $t\,j_x = 500$. This is necessary for relatively smaller chains. However, for larger chains, $t\,j_x = 5$ is a sufficient time of evolution to calculate the average LE as it falls sharply in a small time and remains zero in further evolution.

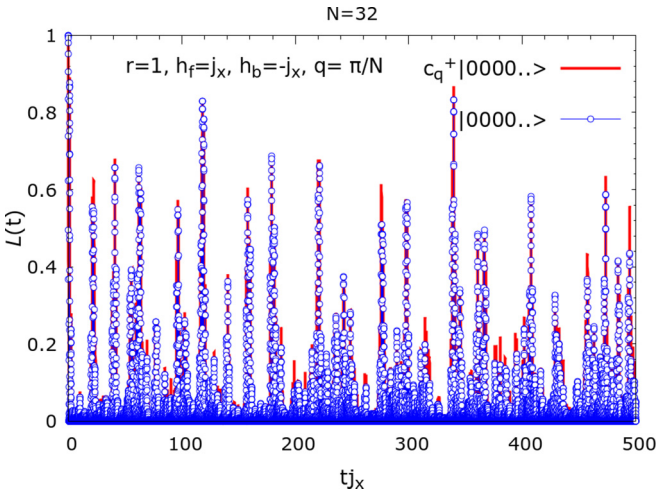

FIG. 5. LE for the one-magnon initial state with a definite momentum. The plot is for $N = 32$ at $r = 1$, $h_f = j_x = -h_b$. The presence of one magnon increases the revival peaks by a smaller amount. However, the increase is distinguishable only for smaller chains.

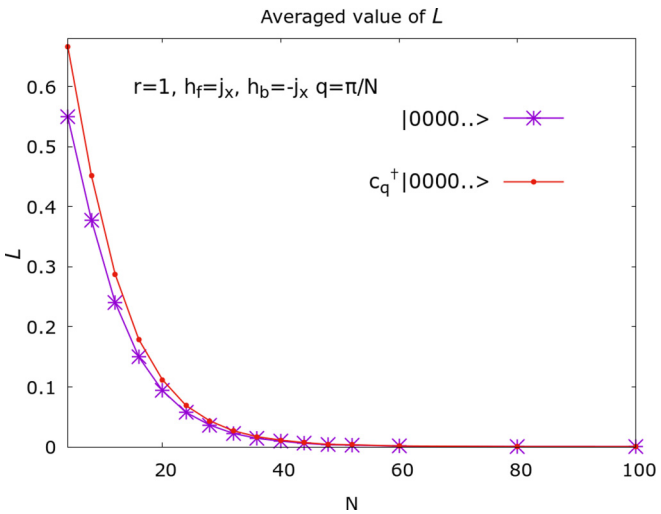

FIG. 6. Averaged values of the LE as a function of chain lengths for two different initial states. The system parameters are $r = 1$, $h_f = j_x = -h_b$. The one-magnon initial state with momentum value, $q = \pi/N$, has frequent revival peaks, which increases the average value of the LE as compared to the LE with a no-magnon initial state.

The plot shows the vanishing gap between LE in two cases as the spin system gets bigger. The stronger revival peaks for the one-magnon initial state places the time-averaged $L(t)$ on the top in the plot. We can see that for $N = 40$ and beyond, the two LE values merge completely, which shows the diminishing effect of a one-magnon excitation in the initial state.

We have seen that for the larger chain lengths, the one-magnon initial state with a definite momentum does not have an impact on the characteristic of $L(t)$. Therefore, we consider $N = 32$ to see the effect produced by it. In Fig. 7, we plot the probability distribution function for the two different mode values separately. In Fig. 7(a), we take $q = \pi/N$ for $N = 32$. We show the results of four values of $k = q - \pi, -q, q, \pi - q$. The probability distribution function $P_q(k, t)$ gives a nonzero distribution only for $k = q$ and it always gives zero for $k \neq q$ even if it belongs to the same mode, i.e., $k = q - \pi, -q, \pi - q$. The probability distribution function remains the same if we shift $q \to \{q - \pi, -q, \pi - q\}$ and take $k = q$ (this is not shown in the plots). This may also be the reason why the probability distribution function goes to zero when $k \neq q$ even within the same mode. The zero probability distribution function means the time-reversal mode state $|\phi'_q(t)\rangle$ and the time-evolved state $|\phi_q(t)\rangle$ remain orthogonal through the evolution. In Fig. 7(b), we choose the last mode value given by $q = (N - 2)\pi/2N$ to show the momentum dependence of the Loschmidt echo. As compared to Fig. 7(a), we can see that the magnitude of the revival peaks depends on the chosen momentum values. However, the peaks of the LE appear at the same time for the different momenta. Also, the Loschmidt echo does not change if we change the sign of momentum in the initial state. This is because q and $-q$ fall in the same mode of the Hamiltonian and we know that the probability distribution functions $P_q(q, t)$ and $P_{q-\pi}(q - \pi, t)$ have the same characteristic.

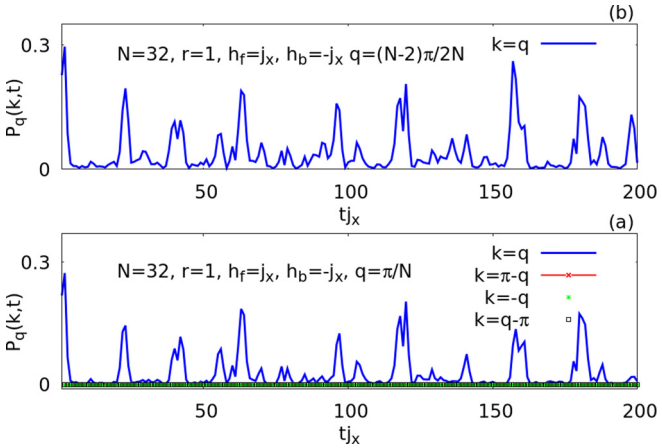

FIG. 7. Plots of the window-averaged probability distribution function values as a function of time for different initial momentum values (a) $q = \pi/N$ and (b) $15\pi/N$, for a spin chain of $N = 32$ at $r = 1$, $h_f = j_x$, $h_b = -j_x$. The window length is equal to 100 time values separated by $\delta t = 0.01 j_x$. The probability distribution for $q \neq k$ gives zero, while for the $q = k$ cases, which is equal to the LE, it shows periodic revivals. For different q in the initial states, the revival peaks of the probability distributions are of different magnitudes, but occur at the same time of the evolution as shown in (a) and (b).

V. ONE-MAGNON INITIAL STATE WITH UNIFORM PROBABILITY DISTRIBUTION

The momentum distribution function of the one-magnon initial state shows a distribution only for the same momentum present in the initial state. This opens the question of what the probability distribution of the momentum would be if the initial state has the excitation of more than one momentum. To investigate this, we consider the initial state to be a one-magnon state with the magnon localized in real space, i.e., $|\psi_1(0)\rangle = c_1^\dagger |00..00\rangle$. In the momentum space, this is an equally probable state for all the allowed momenta of the system. In this section, we consider such an initial state and let this state evolve under the Hamiltonian H_f. The time-reversal state is obtained under the Hamiltonian H_b. The LE is the square of the overlap of two wave functions. For the probability distribution function analysis, we take the overlap of the forward evolved state with a fixed momentum c_k in the initial state and compute the probability distribution of momentum k which may or may not be equal to q. Thus, the initial state is written as

$$|\psi_1(0)\rangle = \frac{1}{\sqrt{N}} \sum_q e^{-iq} c_q^\dagger |00..00\rangle . \tag{19}$$

The evolution of the state can be given by

$$|\psi_1(t)\rangle = \frac{1}{\sqrt{N}} \sum_q e^{-iq} c_q^\dagger(-t) |\psi(t)\rangle , \tag{20}$$

where $|\psi(t)\rangle$ is the state written in Eq. (7). The backward evolution of this state under the Hamiltonian H_b for the same amount of time and taking the overlap with the state $c_k^\dagger |00..00\rangle$ defines the probability distribution function $P(k, t)$ of the momentum k. We also call this function the momentum distribution function. This is written as

$$P(k, t) = \frac{1}{N} | \sum_q e^{-iq} \langle \psi'(t)| c'_k(-t) c_q^\dagger(-t) |\psi(t)\rangle |^2. \tag{21}$$

This can be further simplified by defining $B(k, q) = \langle \psi'(t)| c'_k(-t) c_q^\dagger(-t) |\psi(t)\rangle$. We can rewrite this function as

$$B(k, q) = |A/A_q| C(k, q). \tag{22}$$

And the probability distribution function can now be written as

$$P(k, t) = \frac{1}{N} |A/A_k|^2 |C(k, k) - C(k, k - \pi) + C(k, -k) e^{2ik} - C(k, \pi - k) e^{2ik}|^2. \tag{23}$$

Also, the LE in this case can be written as

$$\mathsf{L}(t) = \frac{1}{N} | \sum_{q,k} e^{-iq} e^{ik} \langle \psi'(t)| c'_k(-t) c_q^\dagger(-t) |\psi(t)\rangle |^2. \tag{24}$$

This can be further simplified in a similar fashion as the probability distribution function. Using the selection for

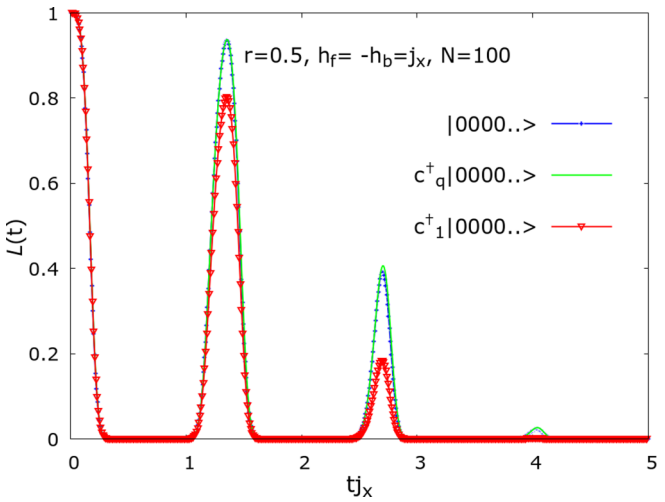

FIG. 8. LE in all the three cases of initial states for $N = 100$ at $r = 0.5$, $h_f = j_x$, $h_b = -j_x$. For the two initial states $|\psi(0)\rangle$ and $|\psi_q(0)\rangle$, the LE almost overlap each other. For the initial state of equally probable momenta, it shows revival peaks of smaller magnitude as compared to the other two cases.

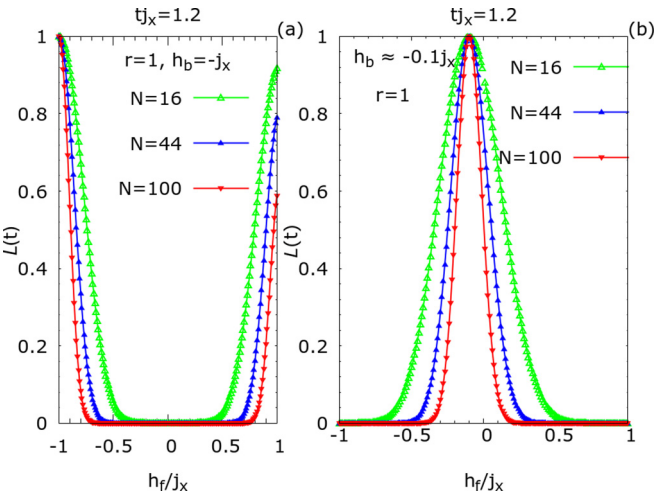

FIG. 9. LE as a function of magnetic field at a fixed time $t j_x = 1.2$ for the different sizes of the system. (a) We consider $r = 1$ and $h_b = -j_x$. The rise of the LE near $h_f = j_x$ shows that the system far away from criticality has the revival peak, which decreases with the system size. (b) We take $h_b = -0.1 j_x$. When the magnetic field in the backward evolution approaches criticality, the revival of the Loschmidt echo is not possible.

momentum values k and q, we can write

$$\mathsf{L}(t) = \frac{1}{N^2}|\sum_k [B(k,k) - B(k,k-\pi) + B(k,-k)e^{2ik} - B(k,\pi-k)e^{2ik}]|^2. \quad (25)$$

To simplify further, we make use of Eq. (22) and write it using the momentum values $k-\pi$, $-k$, k, and $\pi - k$ as

$$\begin{aligned}\mathsf{L}(t) = \frac{1}{N^2}|A|^2|\sum_{0\leqslant k\leqslant \pi/2}\frac{1}{A_k}\{&C(k,k)+C(k-\pi,k)\\ &+C(-k,k)+C(\pi-k,k)-C(k-\pi,k-\pi)\\ &-C(-k,k-\pi)-C(k,k-\pi)-C(\pi-k,k-\pi)\\ &+e^{2ik}[C(k-\pi,-k)+C(-k,-k)\\ &+C(k,-k)+C(\pi-k,-k)-C(k-\pi,\pi-k)\\ &-C(-k,\pi-k)-C(k,\pi-k)\\ &-C(\pi-k,\pi-k)]\}|^2. \end{aligned} \quad (26)$$

Using Eqs. (23) and (26), we calculate the momentum distribution function and the LE, respectively, for the initial state with a flat momentum distribution. For this state, the characteristic of the LE does not change as compared to the no-magnon initial state or the one-magnon initial state with a definite momentum. In Fig. 8, we plot the results for $N = 100$ spins. In this case, the Loschmidt echo does not revive as much as it revives in the other two cases. For no-magnon and one-magnon with definite momentum initial states, the LE plots almost overlap each other. However, the presence of all momenta in the initial state reduces the peaks strengths. For the smaller chains, the difference in the behavior of the LE is a little more pronounced in the long-time evolution. For larger spin chains, the LE remains zero after a certain time. The LE can become zero if the time-evolved states in the forward and reverse evolution become orthonormal. This can alternatively be achieved by tuning the magnetic field and letting the state evolve to some time. We show the behavior of $L(t)$ as a function of the magnetic field in Fig. 9 for the different lengths of the spin chain. In this result, we change the magnetic field in one direction of the evolution, keeping the rest of the parameters fixed. At a specific time $t j_x = 1.2$, at which the revival peak appears, we show the Loschmidt echo as a function of the magnetic field in the forward direction with a fixed value of it in the reverse direction. In Fig. 9(a), we plot at $h_b = -j_x$. We can see that the LE falls to zero when $h_b \to 0$, but revives when $h_b \to j_x$. The revival strengths depend on the length of the chain. In Fig. 9(b), we plot at $h_b = -0.1 j_x$. In this case, we do not see the revival of the Loschmidt echo at all. This justifies the results that we have plotted for the LE so far. It implies that when the system is comfortably far away from the criticality in either direction of the evolution, it can have revival peaks even at the very large system size. However, when the system is set near criticality in one of the directions of the evolution, the revival of the Loschmidt echo is not possible even at lower lengths of the spin chain.

We show the momentum distribution function of Eq. (23) in the full range of k in Fig. 10(a). The four peaks have the same value and they correspond to the momentum values $q - \pi$, $-q$, q, and $\pi - q$. In the initial state with equally probable momenta, overlapping with a state with a definite momentum can have contributions from the four modes states of the state $|\psi_1(t)\rangle$ in Eq. (20), which can have the same momentum. For this reason, we have four peaks in the momentum distribution function plotted against k. The behavior of the momentum distribution depends on the specific time of evolution as well as the length of the spin chain. We have considered the time $t j_x = 1.2$, where the LE shows its first revival peak. The height of the peaks in the probability distribution decreases as the length of the spin chain increases. In Fig. 10(b), the fall of the peaks is plotted as a function of N. The height of the peaks

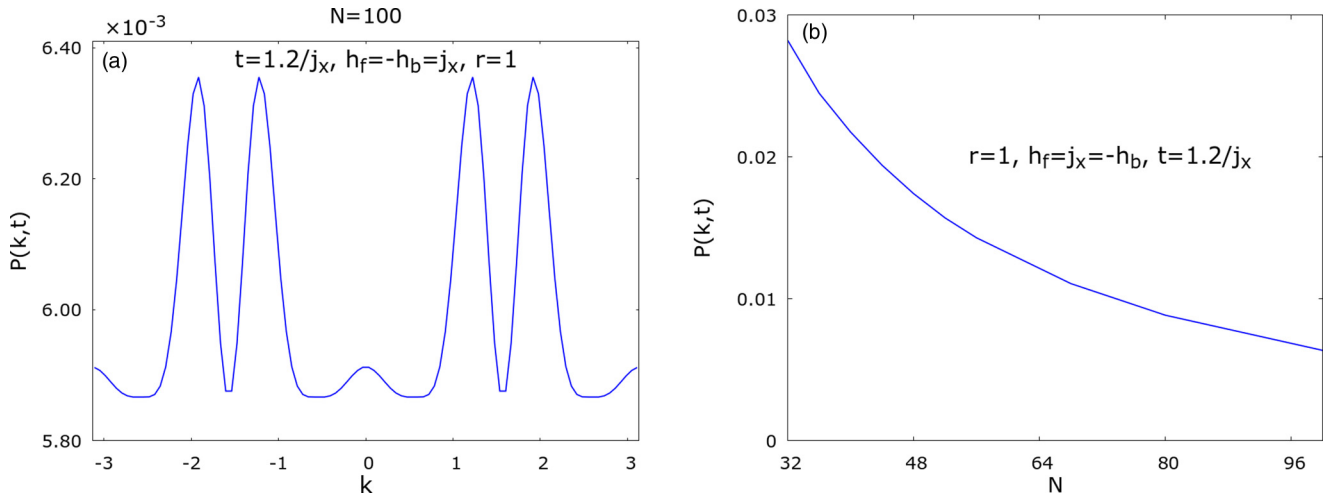

FIG. 10. (a) The probability distribution function as a function of k in the full range at a specific time $j_x t = 1.2$ for $N = 100$. The Hamiltonian parameters are $r = 1$ and $h_f = 1 = -h_b$. The initial state for the state evolution is $|\psi(0)\rangle = c_1^\dagger |00..00\rangle$. The probability distribution function depends on the value of k. It approaches maxima for four values of k. These four peaks' structure basically shows that the probability distribution functions of $P(k-\pi, t)$, $P(-k, t)$, $P(k, t)$, and $P(\pi - k, t)$ as a function of time are the same for a spin chain. (b) The peaks of the probability distribution as a function of N. The peak falls as $1/N$ with size of the chain.

follows a power law as $P(k,t) = 2.177231 * N^{-1.251044}$. We do not show $P(k,t)$ as a function of time as it shows a similar pattern to the LE.

We also show the momentum distribution function for the different time values and also for the different lengths of the spin chain in Fig. 11. The distribution function is plotted in the range of $0 < k < \pi/2$ for two spin chains of length $N = 32$ and $N = 100$ in Figs. 11(a) and 11(b), respectively. For

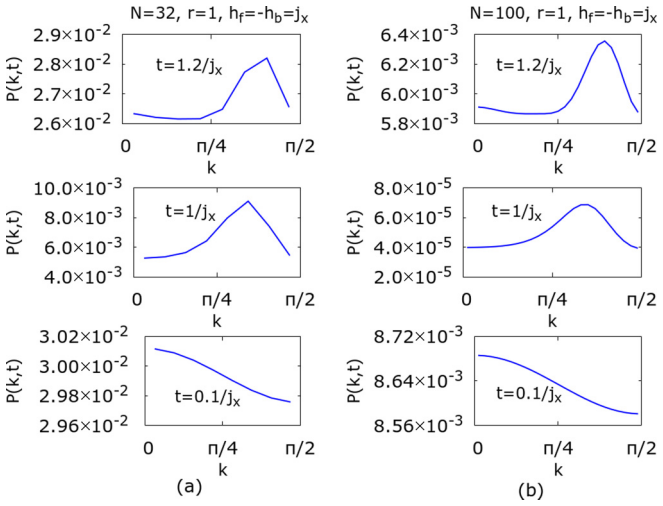

FIG. 11. The probability distribution function as a function of k at the three different times for the two lengths of the chain, (a) for $N = 32$ and (b) $N = 100$. The initial state is $|\psi(0)\rangle = c_1^\dagger |00..00\rangle$. The other parameters are set as $h_f = j_x$, $h_b = -j_x$, and $r = 1$. The range of k has been shortened to plot just one peak of $P(k,t)$. The position of the peak depends on the time of evolution. We can see the peaks near the same k for $t = 1/j_x$ and $t = 1.2/j_x$, while for $j_x t = 0.1$ the peak appears flattened towards $k = 0$. For a larger spin chain in (b), the characteristic of the momentum distribution remains the same; however, the magnitude depends accordingly.

each chain, we consider three different time values $t = 0.1/j_x$, $t = 1/j_x$, and $t = 1.2/j_x$. The Hamiltonian parameters are $r = 1$, $h_f = j_x$ for the forward evolution and $r = 1$, $h_b = -j_x$ for the reverse evolution. In these plots, we have chosen a range of k to show only one peak of the momentum distribution function in any of the plots. Here we can see the time and momentum dependence of $P(k,t)$. The peaks at $t = 1/j_x$ and $t = 1.2/j_x$ are centered around the same value of $k = 1.9$ for $N = 32$ as well as $N = 100$, while for $t = 0.1/j_x$, the peaks are flattened and have shifted towards the left for both chains. Also, we can see that the pattern of the momentum distribution remains the same for different N. However, the magnitude of $P(k,t)$ has fallen as $1/N$ order. The $P(k,t)$ has magnitude of the order of 10^{-2} at $t = 1/j_x$ compared to the other time values. At this moment, the LE is also almost zero, as can be seen in Fig. 8.

VI. LOSCHMIDT ECHO WITH KICKED MAGNETIC FIELD

In previous sections, we discussed the LE for the Hamiltonian under the uniform magnetic field. In this section, we consider the interaction Hamiltonian under the kicked magnetic field, which is introduced using the δ function. In general, the characteristic of the dynamics under this Hamiltonian is similar to the dynamics under the constant magnetic field case. However, the kicks values are determining factor in the dynamics. The special values of kicks give surprising results for the LE. The effect of applying the magnetic field using the δ function occurs only at the kicking times, and, in between the two kicks, the dynamics is governed by the critical Hamiltonian, i.e., Hamiltonian with the zero magnetic field. So, the dynamics has a mixed effect of the critical and noncritical Hamiltonians. This affects the system most when we choose special kick values. The analytical solution of the model has been presented in our previous work [62]. Here,

we review for convenience. In the symbolic form, the constituent terms of the Hamiltonian in Eq. (2) can be written as $H_{xx} = H(j_x, 0, 0)$, $H_{yy} = H(0, j_y, 0)$, and $H_z = H(0, 0, j_z)$. The full Hamiltonian then is given by $H = H_{xx} + H_{yy} + H_z$. The kicked Hamiltonian can be written as

$$H = H_{xx} + H_{yy} + \sum_{n=-\infty}^{\infty} \delta(n - \frac{t}{\tau})h \sum_{i=1}^{N} \sigma_i^z. \tag{27}$$

Here, we apply the magnetic field in the kicked form at period τ. The time after the n kicks is given by $t = n\tau$. The Hamiltonian is periodic over τ. In this case, the dynamics can be governed by the Floquet operator formalism. The Hamiltonian is broken into two parts, namely, the interaction $H_{xx} + H_{yy}$ and the magnetic field H_z Hamiltonians. The unitary operator between the two successive kicks is written as

$$U = e^{-i\tau(H_{xx}+H_{yy})} e^{-i\tau H_z}. \tag{28}$$

And the state after n number of kicks can be written as

$$|\psi_n(t)\rangle = U\,|\psi_{n-1}(t)\rangle = U^n\,|\psi(0)\rangle\,. \tag{29}$$

While considering an unentangled state in the computational basis as an initial state, the evolution can only be governed by the interaction Hamiltonian between the two kicks. The unitary operator with the H_z Hamiltonian can give only a phase contribution as the initial state is an eigenbasis of H_z. The interaction part of the Hamiltonian can be diagonalized for every mode q, which remains associated with the other three momentum values $c_{q-\pi}$, c_{-q}, and $c_{\pi-q}$. However, the two parts of the Hamiltonian do not commute; therefore, it is necessary to transform the H_z in terms of the eigenstates of the interaction Hamiltonian (the explicit calculation of this unitary operator can be seen here [62]). For a mode q, the unitary operator in Eq. (28) can be written in the tensor product form as $U = V_1 \otimes V_2$. The matrices V_1 and V_2 can be expressed and diagonalized in the suitable basis states, $|00\rangle, |01\rangle, |10\rangle, |11\rangle$. We recall the eigenvalues of V_1, which are written as $\lambda_\pm = \frac{1}{2}[(e^{4iet} + 1)\cos(2ht) \pm \sqrt{(e^{4iet}+1)^2\cos(2ht)^2 - 4e^{4iet}}]$ with the corresponding eigenstates, $X_{13}^\dagger\,|00\rangle = x_1\,|10\rangle + y_1\,|01\rangle$ and $Y_{13}^\dagger\,|00\rangle = x_2\,|10\rangle + y_2\,|01\rangle$, where x_i, y_i are the normalized coefficients of the eigenstates. The subscript labels in $X_{13}\,|00\rangle = X_{13}\,|0_1 0_3\rangle$ are the labels on the fermions for our convenience. Similarly, the eigenvalues of V_2 are $\lambda'_\pm = \lambda_\pm(iet \to -iet)$ and the corresponding eigenstates are $X_{24}^\dagger\,|00\rangle = x'_1\,|10\rangle + y'_1\,|01\rangle$ and $Y_{24}^\dagger\,|00\rangle = x'_2\,|10\rangle + y'_2\,|01\rangle$. Thus, the eigenvalues and the corresponding eigenvectors of the unitary U are written as

$$\begin{aligned}
\lambda_1 &= \lambda_+\lambda'_+, \quad |\lambda_1\rangle = X_{13}^\dagger X_{24}^\dagger\,|\text{vacuum}\rangle\,,\\
\lambda_2 &= \lambda_-\lambda'_+, \quad |\lambda_2\rangle = Y_{13}^\dagger X_{24}^\dagger\,|\text{vacuum}\rangle\,,\\
\lambda_3 &= \lambda_+\lambda'_-, \quad |\lambda_3\rangle = X_{13}^\dagger Y_{24}^\dagger\,|\text{vacuum}\rangle\,,\\
\lambda_4 &= \lambda_-\lambda'_-, \quad |\lambda_4\rangle = Y_{13}^\dagger Y_{24}^\dagger\,|\text{vacuum}\rangle\,.
\end{aligned} \tag{30}$$

The vacuum state $|vacuum\rangle$ is a direct product of the vacuum states of the V_1 and V_2 matrices. For each eigenvalue λ_i in Eq. (30), the corresponding eigenvector of U can be rewritten in terms of the momentum operators $c_{q-\pi}$, c_{-q}, c_q, and $c_{\pi-q}$.

We write the first eigenstate of the unitary U as

$$\begin{aligned}
|\lambda_1\rangle = [&\alpha_1 + \alpha_2(c_q^\dagger c_{\pi-q}^\dagger) + \alpha_3(c_{-q}^\dagger c_q^\dagger) + \alpha_4(c_{q-\pi}^\dagger c_{\pi-q}^\dagger)\\
&+ \alpha_5(c_{q-\pi}^\dagger c_q^\dagger) + \alpha_6(c_{q-\pi}^\dagger c_{-q}^\dagger c_q^\dagger c_{\pi-q}^\dagger)]\,|0000\rangle\,,
\end{aligned} \tag{31}$$

where the probability amplitudes $\alpha_i = f(x_i, y_i, x'_i, y'_i)$ are a function of the coefficients of eigenvectors of the matrices V_1 and V_2. The other eigenstates of unitary operator U can be written in a similar way. It is good to recall that the state $|\lambda_i\rangle$ is written for a mode, and the full state of the system is given by the direct product of $N/4$ such modes, as has been expressed in Eq. (7). The eigenstates $|\lambda_i\rangle$ for the kicked Hamiltonian are equivalent to the state $|\phi_q(t)\rangle$ for the direct Hamiltonian case written in Eq. (7). For the kicked Hamiltonian, we can write $|\psi_n(t)\rangle$ and $|\psi'_n(t)\rangle$ for the forward and the reverse evolved state, respectively. We follow the same parameter labels as h_f for the magnetic field in forward evolution, while h_b for the same in reverse evolution. The state after the n kicks of the magnetic field can be written as

$$|\psi_n(t)\rangle = U^n\,|\psi(0)\rangle = \prod_q \sum_{i=1}^{4} \lambda_i^n\,|\lambda_i\rangle\,\langle\lambda_i|\psi(0)\rangle. \tag{32}$$

Using Eq. (32), we compute the Loschmidt echo in the kicked Hamiltonian case for the values of the different parameters. The kicking time of the magnetic field determines the behavior of the LE. For a kick period of infinitesimally small value, the results of the direct Hamiltonian case and the kicked case are the same. At special kicks, the LE shows surprising behaviors. At $\tau = \pi/4$, with Hamiltonian parameters $j_x = j_y = 1$ and $h = j_x$, the wave function does not evolve at all from the initial state $|00..00\rangle$. This can be shown analytically for the spin chain of $N = 4$ sites. For other h/j_x values, the wave functions in the forward and the reverse directions show evolution. However, changing the direction of the magnetic field does not alter the wave function, so the overlap of the $|\psi'_n(t)\rangle$ and $|\psi_n(t)\rangle$ gives unity. Also, it is important to see that after the first kick, the LE is unity. It is because we have considered the same local interaction parameters r in both directions of evolution. The unitary with the magnetic field only changes the phase of the amplitudes of the wave functions, which in overlap do not change the LE. The LE for a smaller spin chain at $\tau = \pi/4$ is plotted in Fig. 12, where it is unity for $r = 1$ and $h/j_x = 1$. For an arbitrary magnetic field value, it shows revivals at arbitrary times during evolution and, as the magnetic field is tuned towards unity ($h/j_x = 0.9$), the peaks become more pronounced only at fewer points in the evolution, which all disappears when the magnetic field is tuned at exactly $h = j_x$. In Fig. 13, we show the LE for the different spin chains at $\tau = \pi/4$, $j_x = j_y = 1$, and $h = j_x$. The reverse field is set at $h_b = 0.9j_x$. We can see that in the long-time evolution, the smaller chains have revival peaks, while for the larger spin chains, the Loschmidt echo falls exponentially and does not show the revival similar to the LE in the direct Hamiltonian case.

In Fig. 14, we show the window-averaged LE at an arbitrary kick $\tau = \pi/12j_x^{-1}$. The window length is set equivalent to 50 kicks. The parameters in the main plot are set as $r = 1$, $h_f = j_x$, and the magnetic field is flipped in the reverse direction of evolution. For a smaller chain $N = 16$, the revival

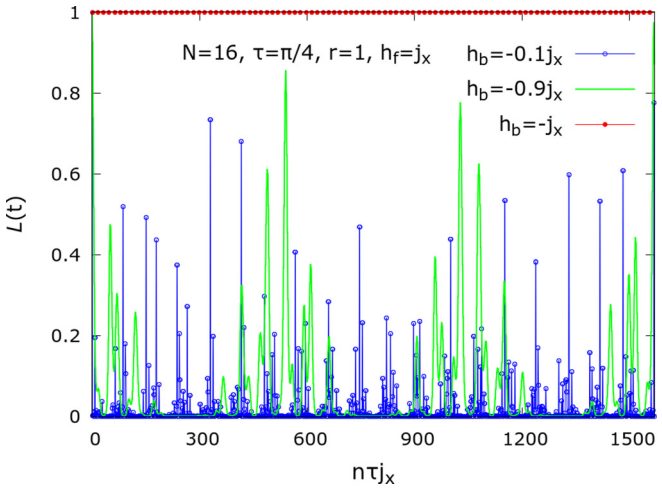

FIG. 12. The LE for a small chain of $N = 16$ at a special kick $\tau = \pi/4$. At $r = 1$, $h_f/j_x = -h_b/j_x = 1$, the system does not show the dynamics. Changing the magnetic field to $h_b \to 0$ in reverse evolution, the LE shows frequent revival peaks. As the magnetic field is tuned towards unity (in $h/j_x \to 1$), the revival peaks are rare but very significant, which subsequently disappear as $h/j_x = 1$.

peaks occur frequently, which gives the window average a higher value of nearly 0.2. However, the number of revival peaks of the Loschmidt echo for larger spin chains significantly reduces, giving a lower window average. For the spin length as large as $N = 100$, the revival peaks of the Loschmidt echo are absent. The inset plot is set at the same parameters as the main plot, except that we consider reverse magnetic field $h_b = 0.1 j_x$. In this case, the LE saturates at the smaller chain length very shortly after the evolution starts and does not revive even at the relatively smaller length of the chain, $N = 44$.

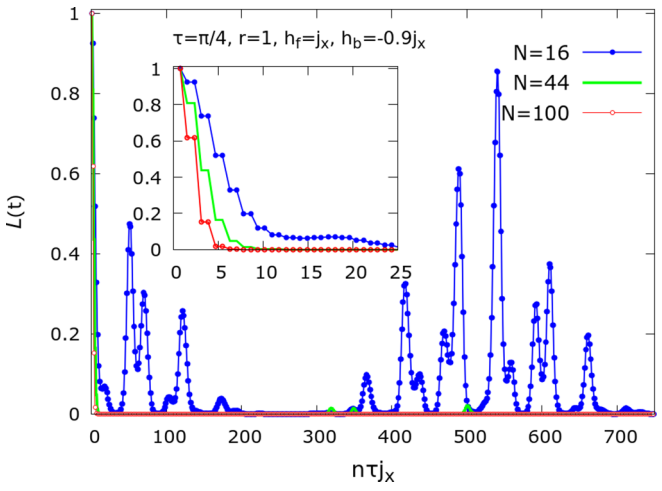

FIG. 13. LE for different chain lengths at $\tau = \pi/4$. For the larger spin chains, similar to the direct Hamiltonian behavior, the LE falls sharply after the evolution begins and does not show revival peaks in the long-time evolution. However, at $\tau = \pi/4$ and $h_f/j_x = -h_b/j_x = -1$, the LE behavior remains the same.

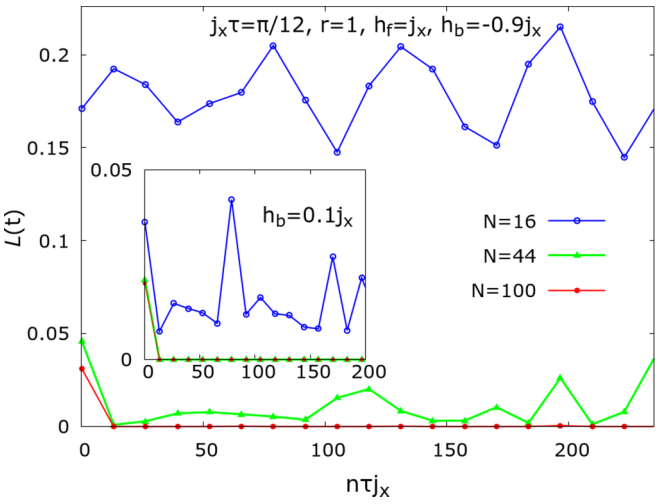

FIG. 14. Window-averaged plots of the LE for the different spin chain lengths. We consider arbitrary $\tau = \pi/12 j_x^{-1}$ and the direction of the magnetic field $h/j_x = 1$ is reversed in reverse evolution. We can see that the LE decreases substantially as the length of the spin chain increases from $N = 16$ to $N = 44$. Also, revival peaks are absent for the larger spin chain. Inset: the magnetic field is set near the critical point in the reverse evolution, which reduces the LE significantly. Also, the LE saturates at smaller spin system $N = 44$ in this case. The window length is considered to be 50 kicks.

VII. CONCLUSION

We have studied the Loschmidt echo in a Kitaev Hamiltonian under the constant and the kicked magnetic fields. The analytical as well as the numerical approach has been applied to compute the LE. We consider different initial states. These states are a no-magnon initial state, a one-magnon initial state with definite momentum, and a one-magnon initial state with a uniform probability distribution. The behavior of LE is analytic throughout the evolution at different parameter values. In the direct Hamiltonian case, we have presented results for two parameter sets: first, when the system is near criticality in either direction of the evolution, and second, when the system is away from the criticality in both directions of the evolution. For smaller chains, the Loschmidt echo periodically shows revival peaks in the long-time evolution. But unlike quantum correlations such as magnetization and concurrences dynamics, the LE does not show the revival peaks in long-time evolution for longer spin chains, although it has a short-time revival peak that is present for longer chains. When the system is at the critical point during forward or reverse evolution, the LE does not have such revival peaks. This behavior can also be seen when we show the LE as a function of the magnetic field. However, near the criticality of the system, the LE can have long-time revival peaks even for the larger chains. This behavior is present only when typically small magnetic fields are present in both directions of the evolutions. These revival peaks occur at different times contrasting with the short-time revival peaks of the LE in a noncritical regime. In the thermodynamic limit, the LE does not show revival peaks irrespective of whether the system is near critical or away from it in either direction of the evolution.

The presence of a magnon with definite momentum in the initial state reduces the revival peaks, which depends on the length of the chain. In longer chains, it does not have a significant effect for the reason that the magnon excitation affects only the evolution of one mode state of the Hamiltonian. Therefore, for sufficiently larger chains, the effect is not seen at all. However, the initial state with equally probable momenta shows a significant drop in subsequent revival peaks even for the longer chains as compared to the revival peaks of the LE with a no-magnon initial state. The presence of momentum in the initial state provides a framework to investigate the probability distributions of different momenta in the evolved state of the system. For the initial state having one-magnon excitation with definite momentum, the probability distribution of a different momentum gives zero even if the momentum belongs to the same mode present in the initial state. The probability distributions for a different momentum in the initial state show the same character during the long-time evolution. However, they have different peak strengths. The probability distribution of the same momentum is equivalent to the LE in this case.

For the initial state of one magnon with a uniform probability distribution, the momentum distribution function of a mode has four peaks when plotted as a function of momentum. These peaks correspond to the associated momenta of the same mode. The momentum distribution is an overlap function with a specific momentum in the initial state, which can give nonzero values when it overlaps with at least four modes states of the evolved state in Eq. (20), which have that specific momentum excitation. This explains the four-peak structure of the momentum distribution function. At specific times, the probability distribution function as a function of the momentum values attains its maximum near $k \approx 1.2$ for different chain lengths when N is large enough, say near $N = 100$. For smaller chain lengths, it differs significantly. The maxima of the probability distribution function fall as the length of the chain increases as $\approx O(1/N)$. This is exactly for the same reason that we have for the initial state of one magnon with definite momentum where the effect of the magnon decreases as the length of the chain increases.

In the last section, we have considered the kicked Hamiltonian case for the Loschmidt echo analysis. The LE generally shows a similar characteristic as the direct Hamiltonian case, except at a few special kick parameters. For a larger spin chain, the LE falls to zero in a few kicks just after the evolution and does not revive, while for a smaller chain, it shows the revival peaks in the long-time evolution. However, in the kicked case, the kick parameter may define the character of the LE. One such special kick we consider is $\tau = \pi/4$, where the evolution of the Hamiltonian does not happen at all, for any length of the chain. This behavior is because of the characteristic of the wave function evolving under the kicked Hamiltonian.

ACKNOWLEDGMENT

V.S. would like to acknowledge the support of SERB under the Matrics scheme.

[1] I. Bloch, J. Dalibard, and W. Zwerger, Many-body physics with ultracold gases, Rev. Mod. Phys. **80**, 885 (2008).

[2] M. Belsley, Ultracold atoms in optical lattices: Simulating quantum many-body systems, by Maciej Lewenstein, Anna Sanpera and Verònica Ahufinger, Contemp. Phys. **54**, 112 (2013).

[3] A. Polkovnikov, K. Sengupta, A. Silva, and M. Vengalattore, Nonequilibrium dynamics of closed interacting quantum systems, Rev. Mod. Phys. **83**, 863 (2011).

[4] A. Mitra, Quantum quench dynamics, Annu. Rev. Condens. Matter Phys. **9**, 245 (2018).

[5] W. H. Zurek, U. Dorner, and P. Zoller, Dynamics of a Quantum Phase Transition, Phys. Rev. Lett. **95**, 105701 (2005).

[6] S. I. Mistakidis, L. Cao, and P. Schmelcher, Negative quench induced excitation dynamics for ultracold bosons in one-dimensional lattices, Phys. Rev. A **91**, 033611 (2015).

[7] S. I. Mistakidis, L. Cao, and P. Schmelcher, Resonant quantum dynamics of few ultracold bosons in periodically driven finite lattices, J. Phys. B: At. Mol. Opt. Phys. **47**, 225303 (2014).

[8] C. Lupo and M. Schiro, Transient Loschmidt echo in quenched Ising chains, Phys. Rev. B **94**, 014310 (2016).

[9] L. Piroli, B. Pozsgay, and E. Vernier, Non-analytic behavior of the Loschmidt echo in *XXZ* spin chains: Exact results, Nucl. Phys. B **933**, 454 (2018).

[10] R. Jafari, Quench dynamics and ground state fidelity of the one-dimensional extended quantum compass model in a transverse field, J. Phys. A: Math. Theor. **49**, 185004 (2016).

[11] H. T. Quan, Z. Song, X. F. Liu, P. Zanardi, and C. P. Sun, Decay of Loschmidt Echo Enhanced by Quantum Criticality, Phys. Rev. Lett. **96**, 140604 (2006).

[12] Z.-G. Yuan, P. Zhang, and S.-S. Li, Loschmidt echo and Berry phase of the quantum system coupled to the *XY* spin chain: Proximity to quantum phase transition, Phys. Rev. A **75**, 012102 (2007).

[13] D. Rossini, T. Calarco, V. Giovannetti, S. Montangero, and R. Fazio, Decoherence induced by interacting quantum spin baths, Phys. Rev. A **75**, 032333 (2007).

[14] J. Häppölä, G. B. Halász, and A. Hamma, Universality and robustness of revivals in the transverse field *XY* model, Phys. Rev. A **85**, 032114 (2012).

[15] S. Montes and A. Hamma, Phase diagram and quench dynamics of the cluster-*XY* spin chain, Phys. Rev. E **86**, 021101 (2012).

[16] F. Igloi and H. Rieger, Quantum Relaxation after a Quench in Systems with Boundaries, Phys. Rev. Lett. **106**, 035701 (2011).

[17] R. Jafari and H. Johannesson, Loschmidt Echo Revivals: Critical and Noncritical, Phys. Rev. Lett. **118**, 015701 (2017).

[18] R. Jafari and H. Johannesson, Decoherence from spin environments: Loschmidt echo and quasiparticle excitations, Phys. Rev. B **96**, 224302 (2017).

[19] K. Najafi and M. A. Rajabpour, On the possibility of complete revivals after quantum quenches to a critical point, Phys. Rev. B **96**, 014305 (2017).

[20] P. Haikka, J. Goold, S. McEndoo, F. Plastina, and S. Maniscalco, Non-Markovianity, Loschmidt echo, and criticality: A unified picture, Phys. Rev. A **85**, 060101(R) (2012).

[21] A. Bayat, S. Bose, H. Johannesson, and P. Sodano, Universal single-frequency oscillations in a quantum impurity system after a local quench, Phys. Rev. B **92**, 155141 (2015).

[22] R. Jafari and A. Akbari, Gapped quantum criticality gains long time quantum correlations, Europhys. Lett. **111**, 10007 (2015).

[23] A. Bayat, B. Alkurtass, P. Sodano, H. Johannesson, and S. Bose, Measurement Quench in Many-Body Systems, Phys. Rev. Lett. **121**, 030601 (2018).

[24] L. Benini, P. Naldesi, R. A. Romer, and T. Roscilde, Loschmidt echo singularities as dynamical signatures of strongly localized phases, New J. Phys. **23**, 023030 (2021).

[25] A. Chenu, I. L. Egusquiza, J. Molina-Vilaplana *et al.*, Quantum work statistics, Loschmidt echo and information scrambling, Sci. Rep. **8**, 12634 (2018).

[26] C.-J. Lin and O. I. Motrunich, Out-of-time-ordered correlators in a quantum Ising chain, Phys. Rev. B **97**, 144304 (2018).

[27] B. Yan, L. Cincio, and W. H. Zurek, Information Scrambling and Loschmidt Echo, Phys. Rev. Lett. **124**, 160603 (2020).

[28] K. A. Landsman *et al.*, Verifed quantum information scrambling, Nature (London) **567**, 61 (2019).

[29] M. K. Joshi, A. Elben, B. Vermersch, T. Brydges, C. Maier, P. Zoller, R. Blatt, and C. F. Roos, Quantum Information Scrambling in a Trapped-Ion Quantum Simulator with Tunable Range Interactions, Phys. Rev. Lett. **124**, 240505 (2020).

[30] M. Blok *et al.*, Quantum Information Scrambling on a Superconducting Qutrit Processor, Phys. Rev. X **11**, 021010 (2021).

[31] X. Mi *et al.*, Information scrambling in quantum circuits, Science **374**, 1479 (2021).

[32] P. G. Sreeram, V. Madhok, and A. Lakshminarayan, Out-of-time-ordered correlators and the Loschmidt echo in the quantum kicked top: How low can we go?, J. Phys. D: Appl. Phys. **54**, 274004 (2021).

[33] R. K. Shukla, A. Lakshminarayan, S. K. Mishra, Out-of-time-order correlators of nonlocal block-spin and random observables in integrable and nonintegrable spin chains, Phys. Rev. B **105**, 224307 (2022).

[34] J. Braumüller, A. H. Karamlou, Y. Yanay *et al.*, Probing quantum information propagation with out-of-time-ordered correlators, Nat. Phys. **18**, 172 (2022).

[35] M. Heyl, A. Polkovnikov, and S. Kehrein, Dynamical Quantum Phase Transitions in the Transverse-Field Ising Model, Phys. Rev. Lett. **110**, 135704 (2013).

[36] M. Schmitt and S. Kehrein, Dynamical quantum phase transitions in the Kitaev honeycomb model, Phys. Rev. B **92**, 075114 (2015).

[37] C. Rylands, E. A. Yuzbashyan, V. Gurarie, A. Zabalo, and V. Galitski, Loschmidt echo of far-from-equilibrium fermionic superfluids, Ann. Phys. **435**, 168554 (2021).

[38] S. Vajna and B. Dóra, Disentangling dynamical phase transitions from equilibrium phase transitions, Phys. Rev. B **89**, 161105(R) (2014).

[39] F. Andraschko and J. Sirker, Dynamical quantum phase transitions and the Loschmidt echo: A transfer matrix approach, Phys. Rev. B **89**, 125120 (2014).

[40] J. N. Kriel, C. Karrasch, and S. Kehrein, Dynamical quantum phase transitions in the axial next-nearest-neighbor Ising chain, Phys. Rev. B **90**, 125106 (2014).

[41] E. Canovi, P. Werner, and M. Eckstein, First-Order Dynamical Phase Transitions, Phys. Rev. Lett. **113**, 265702 (2014).

[42] B. Žunkovič, A. Silva, and M. Fabrizio, Dynamical phase transitions and Loschmidt echo in the infinite-range *XY* model, Philos. Trans. R. Soc. A **374**, 20150160 (2016).

[43] M. Heyl, Dynamical quantum phase transitions: A review, Rep. Prog. Phys. **81**, 054001 (2018).

[44] M. Lacki and M. Heyl, Dynamical quantum phase transitions in collapse and revival oscillations of a quenched superfluid, Phys. Rev. B **99**, 121107(R) (2019).

[45] G. Piccitto and A. Silva, Dynamical phase transition in the transverse field Ising chain characterized by the transverse magnetization spectral function, Phys. Rev. B **100**, 134311 (2019).

[46] T. H. Kyaw, V. M. Bastidas, J. Tangpanitanon, G. Romero, and L. C. Kwek, Dynamical quantum phase transitions and non-Markovian dynamics, Phys. Rev. A **101**, 012111 (2020)

[47] W. C. Yu, P. D. Sacramento, Y. C. Li, and H.-Q. Lin, Correlations and dynamical quantum phase transitions in an interacting topological insulator, Phys. Rev. B **104**, 085104 (2021).

[48] J. C. Halimeh, M. V. Damme, L. Guo, J. Lang, and P. Hauke, Dynamical phase transitions in quantum spin models with antiferromagnetic long-range interactions, Phys. Rev. B **104**, 115133 (2021).

[49] M. Syed, T. Enss, and N. Defenu, Dynamical quantum phase transition in a bosonic system with long-range interactions, Phys. Rev. B **103**, 064306 (2021).

[50] M. Z. Hasan and C. L. Kane, Colloquium: Topological insulators, Rev. Mod. Phys. **82**, 3045 (2010).

[51] X.-L. Qi and S.-C. Zhang, Topological insulators and superconductors, Rev. Mod. Phys. **83**, 1057 (2011).

[52] J. Alicea, New directions in the pursuit of Majorana fermions in solid state systems, Rep. Prog. Phys. **75**, 076501 (2012).

[53] D. I. Tsomokos, A. Hamma, W. Zhang, S. Haas, and R. Fazio, Topological order following a quantum quench, Phys. Rev. A **80**, 060302(R) (2009).

[54] G. B. Halasz and A. Hamma, Topological Rényi Entropy after a Quantum Quench, Phys. Rev. Lett. **110**, 170605 (2013).

[55] N. Leumer *et al.*, Exact eigenvectors and eigenvalues of the finite Kitaev chain and its topological properties, J. Phys.: Condens. Matter **32**, 445502 (2020).

[56] E. L. Hahn, Spin echoes, Phys. Rev. **80**, 580 (1950).

[57] W. K. Rhim, A. Pines, and J. S. Waugh, Time-reversal experiments in dipolar-coupled spin systems, Phys. Rev. B **3**, 684 (1971).

[58] S. Zhang, B. H. Meier, and R. R. Ernst, Polarization Echoes in NMR, Phys. Rev. Lett. **69**, 2149 (1992).

[59] G. Usaj, H. M. Pastawski, and P. R. Levstein, Gaussian to exponential crossover in the attenuation of polarization echoes in NMR, Mol. Phys. **95**, 1229 (1998).

[60] C. M. Sanchez, A. K. Chattah, and H. M. Pastawski, Emergent decoherence induced by quantum chaos in a many-body system: A Loschmidt echo observation through NMR, Phys. Rev. A **105**, 052232 (2022).

[61] V. Kumar Vimal and V. Subrahmanyam, Quantum correlations and entanglement in a Kitaev-type spin chain, Phys. Rev. A **98**, 052303 (2018).

[62] V. Kumar Vimal and V. Subrahmanyam, Magnetization revivals and dynamics of quantum correlations in a Kitaev spin chain, Phys. Rev. A **102**, 012406 (2020).

[63] V. Subrahmanyam, Block entropy for Kitaev-type spin chains in a transverse field, Phys. Rev. A **88**, 032315 (2013).

[64] A. E. Feiguin and F. Heidrich-Meisner, Pairing states of a polarized Fermi gas trapped in a one-dimensional optical lattice, Phys. Rev. B **76**, 220508(R) (2007).

[65] M. Casula, D. M. Ceperley, and E. J. Mueller, Quantum Monte Carlo study of one-dimensional trapped fermions with attractive contact interactions, Phys. Rev. A **78**, 033607 (2008).

[66] T. Papenbrock, Ground-state properties of hard-core bosons in one-dimensional harmonic traps, Phys. Rev. A **67**, 041601(R) (2003).

[67] F. Deuretzbacher, K. Fredenhagen, D. Becker, K. Bongs, K. Sengstock, and D. Pfannkuche, Exact Solution of Strongly Interacting Quasi-One-Dimensional Spinor Bose Gases, Phys. Rev. Lett. **100**, 160405 (2008).

[68] I. Hagymasi, J. Solyom, and O. Legeza, Momentum distribution functions in a one-dimensional extended periodic Anderson model, Adv. Condens. Matter Phys. **2015**, 614017 (2015).

[69] A. Peres, Stability of quantum motion in chaotic and regular systems, Phys. Rev. A **30**, 1610 (1984).

[70] A. Y. Kitaev, Fault-tolerant quantum computation by anyons, Ann. Phys. (NY) **303**, 2 (2003); A. Y. Kitaev and J. Preskill, Topological Entanglement Entropy, Phys. Rev. Lett. **96**, 110404 (2006); G. Baskaran, S. Mandal, and R. Shankar, Exact Results for Spin Dynamics and Fractionalization in the Kitaev Model, *ibid.* **98**, 247201 (2007); H. D. Chen and Z. Nussinov, Exact results of the Kitaev model on a hexagonal lattice: spin states, string and brane correlators, and anyonic excitations, J. Phys. A: Math. Gen. **41**, 075001 (2008).

[71] S. Trebst and C. Hickey, Kitaev materials, Phys. Rep. **950**, 1 (2022).